Desalination and Water Treatment
www.deswater.com

doi: 10.5004/dwt.2020.25322

183 (2020) 404–412
April

A new approach for the preparation of iron oxide-pillared bentonite as adsorbent of dye

Razieh Shayegh, Mohammad Ghorbanpour*

Chemical Engineering Department, University of Mohaghegh Ardabili, Ardabil, Iran, email: Ghorbanpour@uma.ac.ir (M. Ghorbanpour)

Received 16 July 2019; Accepted 6 December 2019

ABSTRACT

In this study, iron-pillared bentonite nanocomposite was prepared by solid-state ion-exchange method as a novel method. Heating was applied during a solid-state substitution of iron from an iron salt powder to calcium ions from bentonite. The synthesized nanocomposites were investigated using scanning electron microscopy, X-ray diffraction, UV-Vis diffusive reflectance spectroscopy and Brunauer–Emmett–Teller method. Finally, the adsorption properties of the nanocomposite using methylene blue dye as a molecule model were measured. The bentonite color was changed through the solid-state ion exchange from white to red. Surface area and pore volume were enhanced by increasing the processing time. The iron-pillared samples showed a significant improvement in the capacity of methylene blue dye removal compared with parent bentonite. The adsorption results showed that the iron-pillared bentonite nanocomposite is an efficient nano-sorbent for the removal of dyes from aqueous solutions.

Keywords: Solid-state ion exchange; Nanocomposite; Bentonite; Adsorbent

1. Introduction

Dye discharged into the environment without pretreatment is an effluent pollutant. Nowadays, dye has been widely used in products, such as fabrics, leather, paper, cosmetics, polymers and foods [1,2]. The presence of dyes in effluents, even in low concentrations, is a major concern because they are highly visible, toxic to microorganisms and harmful to human health [3]. Recently, removing dyes from wastewater has gained researchers' attention and various methods have been developed, such as chemical oxidation, biodegradation, membrane separation, electrochemical processes, coagulation/flocculation and adsorption [4–7]. Among these methods, adsorption is considered an effective way to remove dyes from wastewater, since it is not destructive and easy to apply. In this sense, the characteristics of the adsorbent surface are important. Metal nanooxides have recently been applied to remove heavy metals and dyes from water and wastewater [10,11]. For instance, iron oxide nanoparticles are an efficient adsorbent [12,13]. Iron-pillared clays are one of the most widely studied nanocomposites among the new group of developed micro porous materials with high surface area [12,14–16]. An important benefit of using these materials is intercalating different active oxide species by clay layers equipped with nanoparticles [14]. The first and most common method in the preparation of metal oxide–pillared clays is the ion exchange process, which comprised of the following three steps: polycation synthesizing by polymerization; next, intercalation of the polycation into layer space of the clay; and finally, applying heat treatment. When heated to a temperature greater than 573 K, the intercalated metal hydroxy cations undergo dehydration and dehydroxylation and are converted to metal oxide clusters acting as pillars to prop the clay layers apart, thus creating a stable micro porous system in the interlamellar space of clay particles [13,17]. The negative outcome

* Corresponding author.

of the ion exchange process is its lengthy processing and multistep preparation procedures [18]. In this research, to resolve these problems, for the first time, a new method titled as "solid-state ion exchange method" was applied.

In solid-state ion exchange method, iron salt is mixed with bentonite and heated around the melting point of iron salt. Diffusion of iron into bentonite was accomplished by substitution of iron with exchangeable calcium of bentonite [19–21]. Synchronized application of heat with ion exchange creates a fast process. Furthermore, under the common procedure, the usual temperature is 300°C, while in this research the reaction was accomplished at 100°C [18,22]. Recent research has produced antibacterial nanocomposites by solid-state ion exchange [23]. However, as far as this study concerns, the present report is the first study on the preparation of iron oxide-pillared bentonite by solid-state ion-exchange method in dye adsorption.

2. Materials and methods

2.1. Materials

Bentonite clay, used as a solid support for iron oxide, was obtained from Kany Saz Jam Company (Rasht, Iran). Prior to the experiments, the bentonite was sieved to give a particle size of roughly 38 μm. The Methylene blue dye was used as the model adsorbate. Methylene blue (MB) is a cationic dye. All aqueous solutions were prepared with deionized water. All reagents were of analytical grade and were used as received without further refinement.

2.2. Synthesis of iron-pillared bentonite nanocomposite

Bentonite was immersed in molten salt, $FeCl_2.\ xH_2O$, at 100°C for 0.5, 1, 2, 3 and 5 min. This operation was undertaken using 5 g of bentonite and 5 g of $FeCl_2.\ xH_2O$. After ion exchange, the bentonite was adequately washed with distilled water and sonicated. This step was intended to remove any compounds that were not diffused in the bentonite structure. After filtration, the obtained composites were dried in an oven for 24 h at 25°C.

2.3. Characterization

X-ray diffraction (XRD) patterns of the samples were characterized using an X-ray diffractometer (Philips PW 1050, The Netherlands) with CuKα radiation (λ = 1.5418 Å, 40 kV and 30 mA, 2θ from 0 to 80° and 0.05° step). The microstructures of the samples were observed through a scanning electron microscope (SEM; LEO 1430VP, Germany).

A Micromeritics Brunauer–Emmett–Teller *(BET)* surface area and porosity analyzer (Gemini 2375, Germany) was used to evaluate the products with N_2 adsorption/desorption at the constant temperature of 77K in the relative pressure range of 0.05–1.00.

A transmission electron microscope (TEM; Philips CM120, Germany) was used to characterize the Fe_yO_x/bentonite composite with respect to its particle size and shape.

Absorption spectra of nanocomposites were measured by a UV-Vis diffusive reflectance spectrophotometer (DRS; Scinco S4100, Korea) at the wavelength range of 200–700 nm.

2.4. Leaching test

The concentrations of Fe ions released from the nanocomposite were determined by atomic absorption spectrometer (AA800, PerkinElmer). For each composite, 0.2 g was immersed in 10 mL of distilled water and vigorously agitated in a shaking water bath (30°C, 200 RPM) for 24 h. Supernatants from each test tube were collected by centrifugation at 4,000 rpm for 10 min. Iron ions released from the nanocomposites were qualitatively determined.

2.5. Adsorption experiments

Batch adsorption experiments were carried out in a set of glass flasks (30 mL) containing 10 mL of MB solutions (50 mg/L) at 298 K, and 0.1 g of each adsorbent added to each solution. The MB solutions were kept under stirring using a mechanical stirrer at 250 rpm. Aliquots of 0.1 mL were withdrawn from the solutions over a period of 4 h, at predetermined time intervals during each run. These aliquots were then diluted, homogenized and centrifuged before the measurement of the supernatant absorbance.

The absorbance was measured using a UV–Vis spectrophotometer (Varian Cary 50 Bio UV–Vis spectrophotometer, USA) to monitor the absorbance at λ_{max} = 664 nm, corresponding to the maximum absorbance. The MB concentrations were each time estimated from a previously prepared calibration curve obtained by plotting the absorbance against the MB concentration of the solution. The batch adsorption was conducted for a contact period of 4 h, time sufficient for the concentration of the solutions to reach a constant value.

The amount of MB adsorbed by adsorbent in each time interval, t, was calculated through the following mass balance equation:

$$q_t = \left(C_0 - C_t\right)\frac{V}{m} \tag{1}$$

where C_0 is the initial liquid-phase MB concentration (mg/L); C_t is the liquid-phase MB concentration at time t (mg/L); V is the volume of the MB solution (10 mL) and m is the mass of adsorbent used (0.1 g).

3. Results and discussion

3.1. Solid-state ion exchange method

The solid-state ion exchange was carried out on the base of sodium and calcium. In this regard, cations in the bentonite structure as a cation exchange were replaced with iron. The following equation describes this point:

$$\text{Bentonite} - Ca^{2+} + FeCl_2 \rightarrow \text{Bentonite} - Fe + CaCl_2 \tag{2}$$

Consequently, high temperature resulted in changing the replaced iron ions to iron oxide nanoparticles.

$$\text{Bentonite} - Fe + O_2 \rightarrow \text{Bentonite} - Fe_yO_x \tag{3}$$

Appearance and color of the parent bentonite was white. Solid-state ion exchange of the bentonite by $FeCl_2$ changed

its color (Fig. 1). By increasing solid-state ion exchange process time at a constant temperature, the color of bentonite changed more. After 30 s of solid-state ion exchange, the color of the sample became light cream. After 1 min, the color was altered to dark cream, creamy brown in 2 min and, finally, after 5 min changed to red. It may be concluded that the color variation is due to the different particle sizes and the amount of metal loaded to the bentonite [23,24]. According to the rules of mass transfer, penetration of iron in the surface layers of bentonite is faster and in deeper layers is more difficult. Here, penetration occurs so that first, iron ions substitute with calcium in the surface layers of the bentonite, and then penetrate to the deeper layers of bentonite.

3.2. DRS spectra

To identify the presence of Fe^{3+} in iron-pillared bentonite nanocomposite, UV–Vis spectra were used; the results of which are illustrated in Fig. 2. It is observed that the maximum absorption of parent bentonite is around 317 nm. After the ion exchange process, this peak was enhanced and shifted to higher wavelengths, which was related to the formation of the nanocomposite. On the other hand, according to the published researches, absorption in wavelength smaller than 300 nm, between 300 and 400 nm and higher than 400 nm was associated with the isolated Fe^{3+}, oligomeric clusters of Fe_xO_y and large Fe_2O_3 particles, respectively [25,26]. Furthermore, absorption at visible range (>450 nm) may be due to d–d transitions, which corresponds to the formation of α-Fe_2O_3 particles [27]. Thus, Fe_2O_3 particles were formed in iron-pillared bentonite nanocomposite when prepared at longer times.

3.3. Morphology

The morphology of natural bentonite and the prepared composites at different ion exchange times was studied, and the SEM images are shown in Fig. 3. In Fig. 3a, bentonite displays a leafy sheet surface texture with a loose and porous microstructure, a typical morphological characteristic of such material. After ion exchange, the structure of the parent bentonite displays some changes. However, the composite prepared at 30 s shows approximately similar structure to 1 min (Fig. 3b); the only difference is that

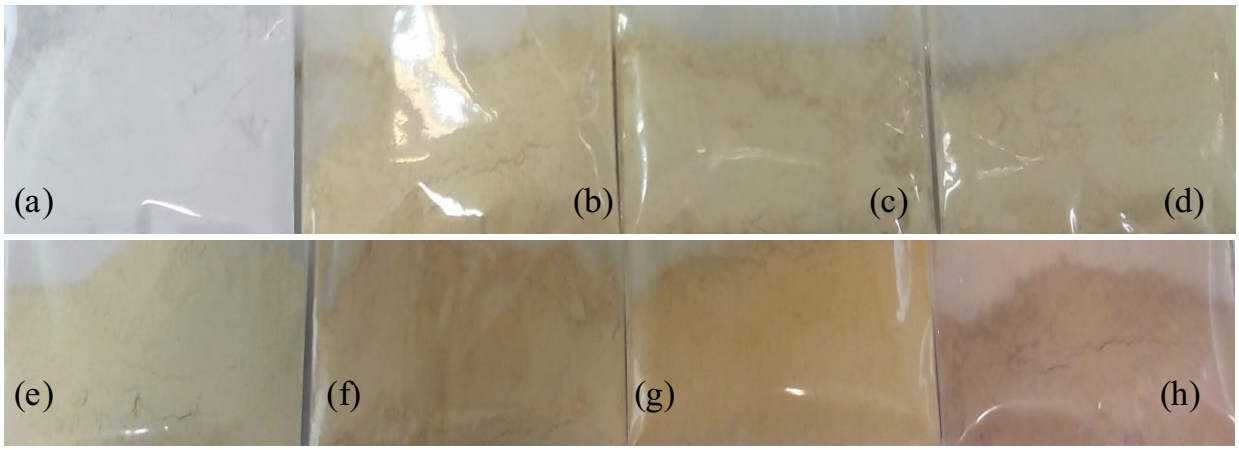

Fig. 1. Photography of the ion exchanged bentonite for (a) 0, (b) 0.5, (c) 1, (d) 1.5, (e) 2, (f) 3, (g) 5 and (h) 10 min.

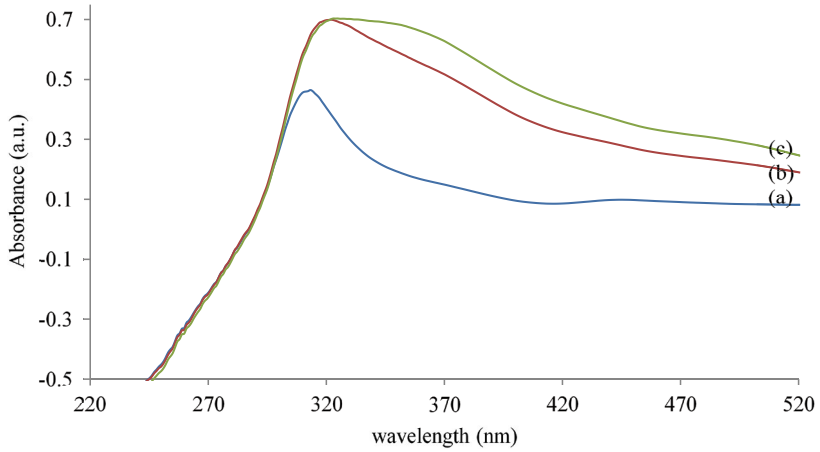

Fig. 2. DRS spectra of parent bentonite (a) and Fe-exchanged bentonite nanocomposite prepared by solid-state ion exchange method for 1 min (b) 1 and 2 min (c).

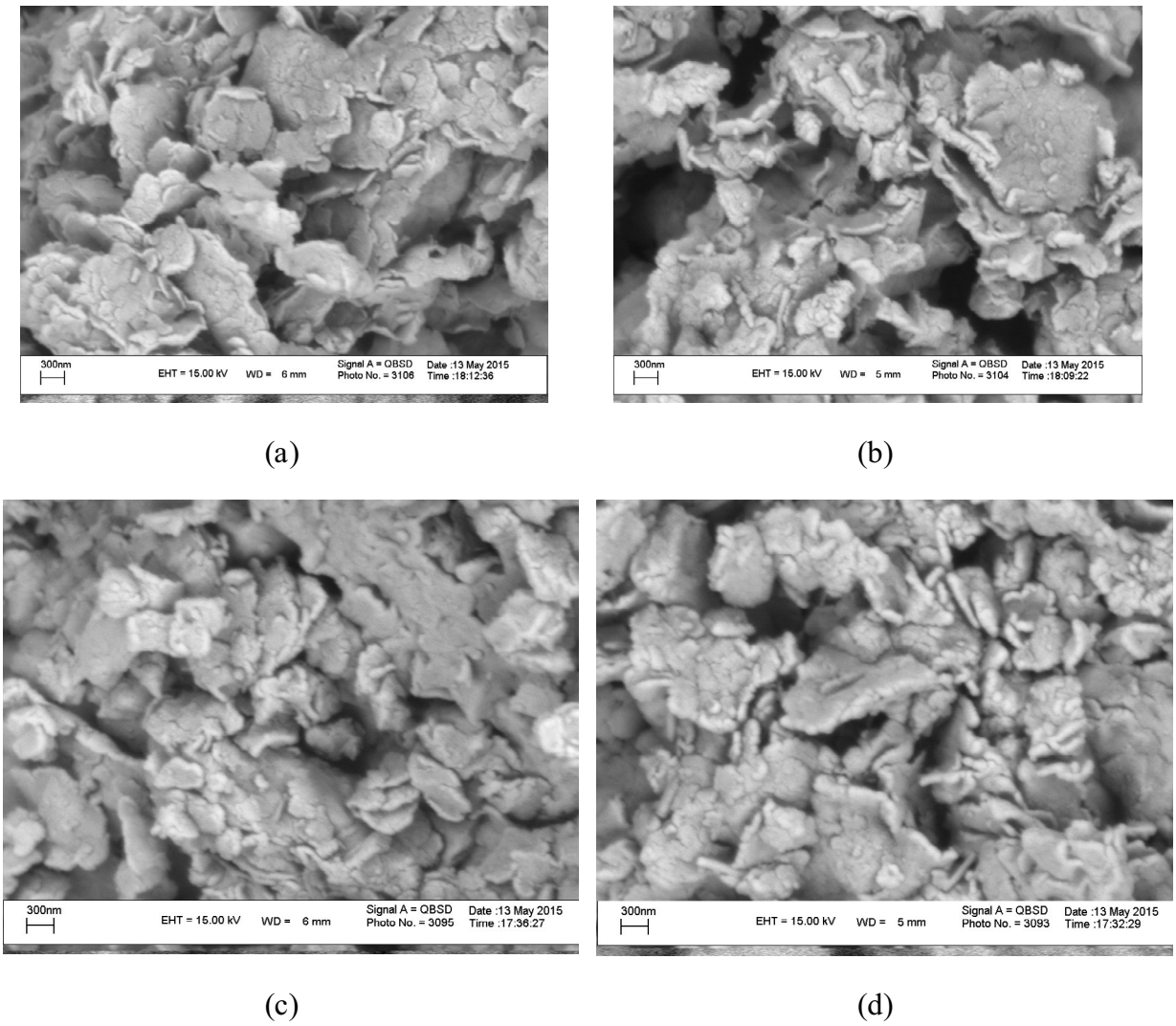

Fig. 3. SEM images of parent bentonite (a) and iron exchanged bentonite nanocomposite prepared by solid-state ion exchange method for 1 (b), 2 (c) and 5 min (d).

the edges of the leafy sheets of bentonite seem to become thicker. Increasing time to 1 min resulted in thicker sheets. It also seems that by immobilizing the iron, porosity between the sheets has declined. However, more processing time resulted in expanding the layers, and the distance between the sheets increased (Figs. 3c and d).

For further investigation, TEM was conducted for the sample prepared at 1 min (Fig. 4). Fig. 4a was taken from the middle part of the sheet, and shows some small separated nanoparticles, whereas, the image of the edge of a sheet illustrates more nanoparticles, which are interconnected (Fig. 4b). This implies that the iron immobilization caused the changing surface structural alterations, followed by intercalation of iron particles into the inner layers of the bentonite [28].

3.4. XRD analysis

Fig. 5 shows the XRD pattern of pure bentonite and iron-pillared bentonite nanocomposite at different times. A typical pattern was observed for bentonite, with an intense $2\theta = 6.27$ reflection relative to the basal spacing d_{001} (1.44 nm). The other reflections correspond to montmorillonite's crystalline structure (2θ = 19.84°, 20.87°, 26.68°, 27.65°, 32.47°, 34.90°, 50.23°, and 60.13°) [13,15]. These peaks appear in the patterns of all the nanocomposites. After ion exchange, the original d spacing in the montmorillonite clay decreased to 1.29 nm for 0.5 min, due to the loss of water initially present in the interlayers.

However, the diffractograms show more differences; by enhancing the process time, the d spacing of interlayers increased and reached 1.38 nm for 2 min sample. It has been also reported that high temperature affected the interlayer structure [29]. Therefore, the peaks of montmorillonite and in ion exchanged samples became broader and less intense. The different d-spacing position and shape of the (001) reflection suggest the introduction of iron nanoparticles within the interlayer structure [13]. Some reported data showed higher d-spacing after ion exchange, compared with bentonite [17,28]. The reason may be due to using a salt solution

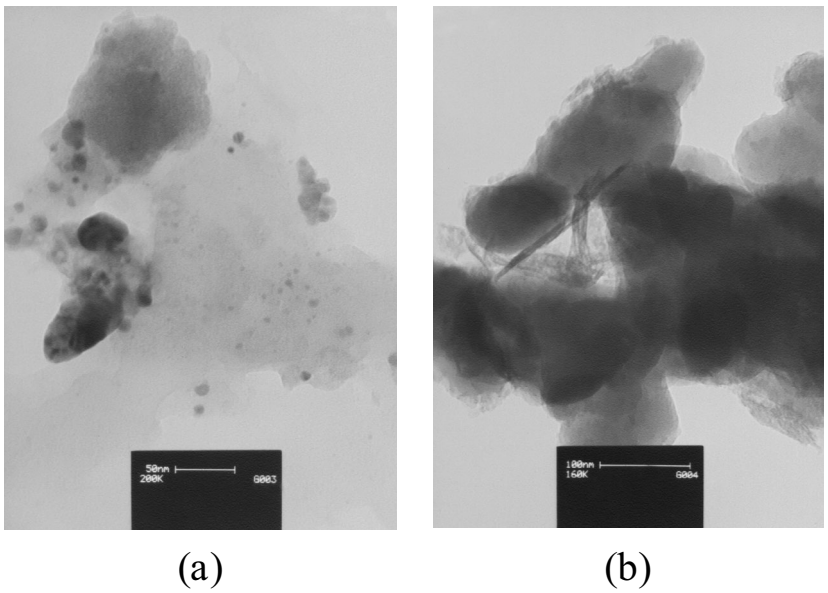

Fig. 4. TEM images of iron exchanged bentonite nanocomposite prepared by solid-state ion exchange method for 1 min.

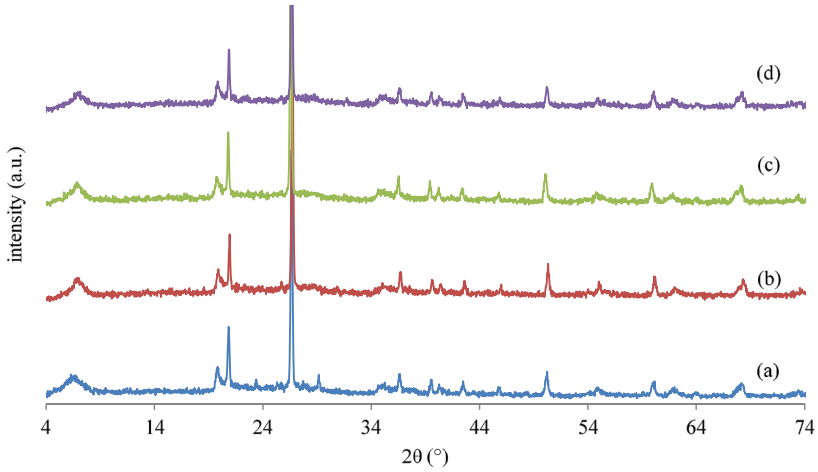

Fig. 5. XRD pattern of parent bentonite (a) and of iron exchanged bentonite nanocomposite prepared by solid-state ion exchange method for 0.5 (b), 1 (c) and 2 min (d).

for the process of ion exchange, which increased the number of ions between the layers, resulting in swollen bentonite. In this study, *d*-spacing of the products, even after 5 min, is less than in the parent bentonite. Here, there are two reasons: the reaction is accomplished in a solid phase, and the high process temperature evaporates the moisture between the layers.

3.5. BET specific surface area analysis

A comparison of adsorption–desorption N_2 isotherms for iron-pillared bentonite nanocomposite by BET analysis was carried out, and the results are provided in Table 1. At first, the bentonite sample had 180 m^2/g porosity. After 1 min, porosity was decreased to 123 m^2/g. It seems that the reason is diffusion of iron ions to the bentonite. Furthermore, at the beginning of ion exchange process, Fe ions penetrate into bentonite layers. Because of the positive charges of Fe ions, the distance between the layers decreases. By increasing ion exchange time, porosity was in the range of 202–221 m^2/g. Given the XRD and SEM results, the porosity of

Table 1
BET analysis of pure bentonite and iron exchanged bentonite nanocomposite

Sample	Surface area (m^2/g)
Bentonite	180
1	123
2	211
3	202
5	221

nanocomposite can be enhanced by the opening of the bentonite's flakes. Another reason may be the oxidation of iron after ion exchange process which is bigger than iron.

3.6. Leaching test

Because the final application of these composites is in water treatment, their stability in water was evaluated. Table 2 shows that the maximum concentration of released Fe was 1.66 mg/l, recorded from nanocomposite synthesized in 4 min. The obtained results indicate that the amount of released iron from these products poses no danger to drinking water. This can be attributed to the permanent attachment of the diffused iron to the bentonite matrix. The advantage of this finding is that the adsorption property of iron-pillared bentonite composite would be longer.

3.7. Adsorption study

The results obtained from adsorption study for removal of methylene blue dye are depicted in Fig. 6. The data show that the samples synthesized in 1 min have better absorption activity compared with the parent bentonite and other samples. Parent bentonite retrieved reduced the solution's dye concentration from 50 to 20 ppm. In other words, 60% of the dye had been removed. The sample produced in 30 s had similar action with bentonite, while the sample of 1 min lowered the concentration to 10 ppm (80% removal efficiency). This phenomenon was attributed to the fact that iron nanoparticles introduced into the interlayers of bentonite, and the agglomeration of nanoparticles was inhibited, meaning that more and more active sites of iron exchanged bentonite nanocomposite could be provided than that of bentonite or nanoparticles. Consecutively, a large number of negative charges on the surfaces of nanocomposite could contribute to the binding of cationic dye (methylene blue).

Table 2
Leaching of iron from parent bentonite and prepared nanocomposites

Time of solid-state ion exchange method (min)	Iron concentration in water (ppm)
0	0.19
0.5	0.22
1	0.51
2	0.59
3	1.66
5	1.62

By increasing processing time to 2 min and beyond, dye removal activity decreased to 60%. According to the DRS results, at the beginning of ion exchange, the majority of doped irons are in the form of ions, and their size is small. Hence, their absorption capacity is high. Then, more iron converts to Fe_2O_3 and consequently, the size of particles increases.

To show the results of adsorption equilibrium and measuring the adsorption rate in different situations, adsorption equilibrium models are used. Equilibrium data of MB adsorption by nanocomposite using two models of Langmuir and Freundlich have been explored. The equations employed in fitting the experimental data in the two models are expressed as Eqs. (4) and (5), respectively:

$$q_e = K_F C_e^n \tag{4}$$

$$q_e = \frac{q_m K_L C_e}{1 + K_L C_e} \tag{5}$$

In the equations, q_e is the equilibrium dye concentration on adsorbent; C_e is equilibrium concentration of dye in aqueous phase; K_F is the Freundlich adsorption constant related to adsorption ability; n is an empirical parameter associated with adsorption intensity; K_L is the Langmuir adsorption constant connected to the affinity of binding sites and q_m is the maximum adsorption capacity of adsorbent.

The adsorption isotherm parameters are listed in Table 3. The results of modeling data equilibrium indicated that the Langmuir isotherm model better estimated the equilibrium

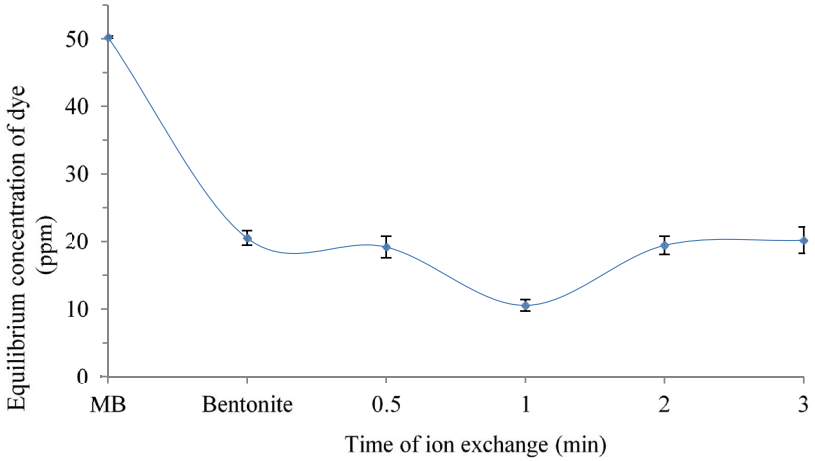

Fig. 6. Amount of MB adsorbed by parent bentonite and iron exchanged bentonite nanocomposites (experimental condition: adsorbent dosage 0.1 g, initial concentration 10 mg/L, sample volume 10 mL, temperature 25°C).

data than did the Freundlich model (Fig. 7). Table 3 shows the maximum adsorption capacity to be 161.3 mg/g for bentonite adsorbent and 200.0 mg/g for bentonite/iron nanocomposite. In other words, the synthesized nanocomposite increased removal capacity up to 25%. According to the previous results, adsorption isotherms of iron-pillared clay were investigated, and the results of the experiment best fitted the Langmuir model [18,22]. Gao et al. [28] investigated the positive effect of ion exchanged bentonite with iron on Rhodamine B absorption and reported the maximum adsorption capacity and Langmuir adsorption constant were 168.13 mg g^{-1} and 1.33 L mg^{-1}, respectively. Furthermore, Cottet et al. [3] evaluated the effect of iron ion exchange on adsorption of montmorillonite. Their results showed that the maximum adsorption capacity and Langmuir adsorption constant were 70 mg g^{-1} and 0.05 L mg^{-1}, respectively [3]. In these two works, there is no information about the initial adsorption of used raw material, although the maximum adsorption capacity and Langmuir adsorption constant of our study is much higher.

Table 3
Adsorption isotherm parameter of methylene blue dye

	Langmuir model			Freundlich model		
	K_l (L/mg)	q_m (mg/g)	R^2	K_f (mg/g)	n	R^2
Bentonite	0.251	161.3	0.98	47.7	2.78	0.99
Iron exchanged bentonite for 1 min	3.33	200.0	0.99	127.2	5.1	0.71

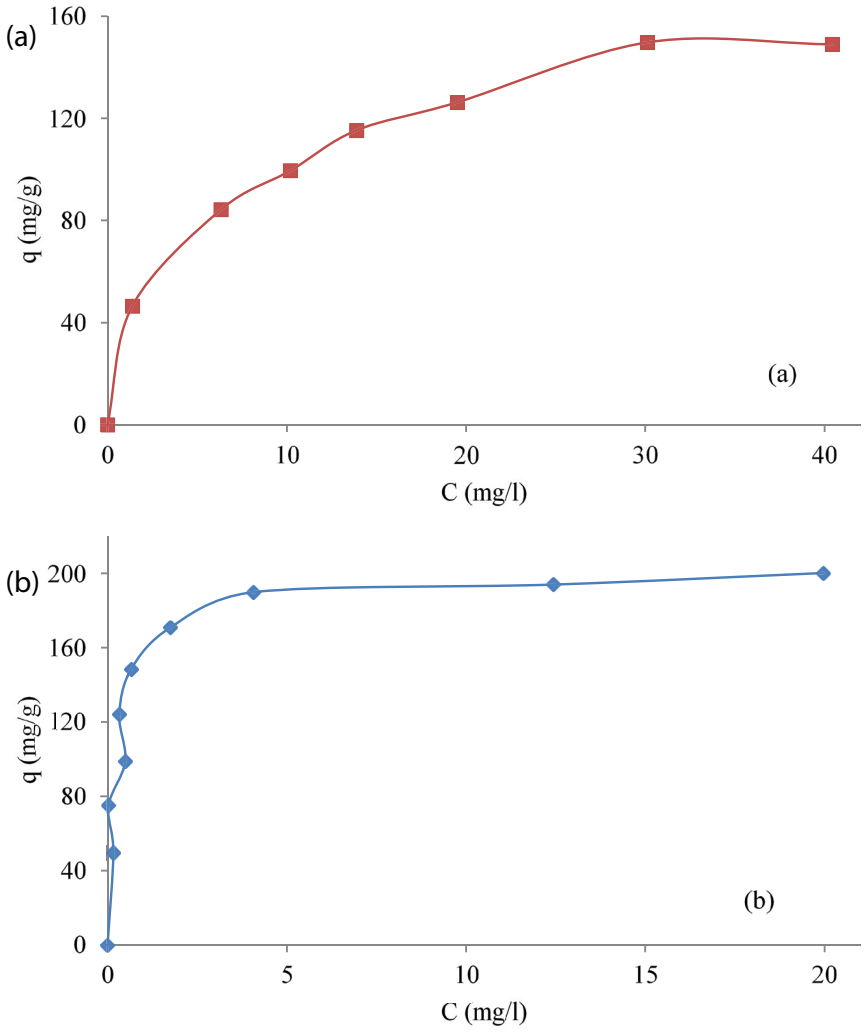

Fig. 7. Langmuir isotherm for adsorption of methylene blue dye on (a) bentonite and (b) iron exchanged bentonite for 1 min (experimental condition: adsorbent dosage 0.1 g, initial concentration 0–100 mg/L, sample volume 10 mL, temperature 25°C).

Table 4
Kinetic parameters of adsorption of methylene blue (experimental condition: adsorbent dosage 0.1 g, initial concentration 50 mg/L, sample of volume 10 mL, temperature 25°C)

	Pseudo-first order			Pseudo-second order		
	q_e (mg/g)	k_1 (mg/g min)	R_1^2	q_e (mg/g)	k_2 (hgm/g)	R_2^2
Bentonite	3.7	0.53	0.69	13.2	0.26	0.99
Exchanged bentonite for 1 min	2.17	0.66	0.60	19.2	0.13	0.99

To evaluate the process of MB adsorption by the nanocomposites, a pseudo-first order model and a pseudo-second order model were applied. These two models are frequently used to describe adsorption in solid–liquid systems. Eqs. (6) and (7) represent the linear forms of the pseudo-first and pseudo-second order kinetics, respectively, after integrating the differential equations.

$$\ln\left(q_e - q_t\right) = \ln q_t - k_1 t \tag{6}$$

$$\frac{t}{q_t} = \frac{1}{k_2 q_e^2} + \frac{1}{q_e} \tag{7}$$

where q_e and q_t are the amounts of adsorbed MB (mg/g) in equilibrium, and t (h) is contact time of adsorption; k_1 (h^{-1}) and k_2 (g/mg h) are the pseudo-first and pseudo-second order rate constants, respectively. If these kinetic models are applicable, the plot of $\ln(q_e - q_t)$ vs. t, and t/q_t vs. t should give a linear relationship, allowing determination of the k_1 and k_2 constants from the slope of the straight lines. The best model is chosen by considering the linear regression correlation coefficient value closest to 1.00 (R_1 for pseudo-first order or R_2 for pseudo-second order).

The kinetic parameters of the pseudo-second and pseudo-first order kinetic models, based on Eqs. (6) and (7) are shown in Table 4. By comparing the correlation coefficient of this equation, it was found that the pseudo-second order model has a better fit. Clearly, the high values of R_2 indicate that the adsorption data conform well to pseudo-second order kinetics.

4. Conclusion

In this research, iron-pillared bentonite nanocomposite was successfully synthesized. The bentonite color changed through the solid-state ion exchange from white to red. The surface area and pore volume were enhanced by increasing the processing time. The results demonstrated that 1 min process time produced an iron oxide-pillared bentonite with greater absorption activity, which was than the Freundlich model. The maximum adsorption capacity is 161.3 mg/g for bentonite absorbent and 200.0 mg/g for bentonite/iron nanocomposite. The results of modeling the data equilibrium indicated that the Langmuir isotherm model estimated the equilibrium data better than the mg/g for the bentonite/iron nanocomposite. In other words, the synthesized iron oxide-pillared bentonite nanocomposites increased the removal capacity up to 25%. By comparing the correlation coefficient of these equations, it was found that the pseudo-second order model has a better fit. These results showed that the iron-pillared bentonite nanocomposite is an efficient nano-sorbent for removing dyes in the aqueous solutions.

References

[1] M.T. Yagub, T.K. Sen, S. Afroze, H.M. Ang, Dye and its removal from aqueous solution by adsorption: a review, Adv. Colloid Interface Sci., 209 (2014) 172–184.

[2] T. Santhi, S. Manonmani, Malachite green removal from aqueous solution by the peel of *Cucumis sativa* fruit, Clean–Soil Air Water 39 (2011) 162–170.

[3] L. Cottet, C.A.P. Almeida, N. Naidek, M.F. Viante, M.C. Lopes, N.A. Debacher, Adsorption characteristics of montmorillonite clay modified with iron oxide with respect to methylene blue in aqueous media, Appl. Clay Sci., 95 (2014) 25–31.

[4] Ç. Üzüm, T. Shahwan, A.E. Eroğlu, K.R. Hallam, T.B. Scott, I. Lieberwirth, Synthesis and characterization of kaolinite-supported zero-valent iron nanoparticles and their application for the removal of aqueous Cu^{2+} and Co^{2+} ions, Appl. Clay Sci., 43 (2009) 172–181.

[5] M. Ghorbanpour, B. Hakimi, A. Feizi, A comparative study of photocatalytic activity of ZnO/activated carbon nanocomposites prepared by solid-state and conventional precipitation methods, J. Nanostruct., 8 (2018) 259–265.

[6] N. Garshasbi, M. Ghorbanpour, A. Nouri, A. Lotfiman, Preparation of zinc oxide-nanoclay hybrids by alkaline ion exchange method, Braz. J. Chem. Eng., 34 (2017) 1055–1063.

[7] S.K. Isalou, M. Ghorbanpour, Catalytic activity of Fe-modified bentonite in heterogeneous photo-Fenton process, Desal. Wat. Treat., 162 (2018) 376–382.

[8] T. Robinson, G. McMullan, R. Marchant, P. Nigam, Remediation of dyes in textile effluent: a critical review on current treatment technologies with a proposed alternative, Bioresour. Technol., 77 (2001) 247–255.

[9] S. Rasalingam, R. Peng, R.T. Koodali, An insight into the adsorption and photocatalytic degradation of rhodamine B in periodic mesoporous materials, Appl. Catal., B, 174 (2015) 49–59.

[10] M. Ghorbanpour, A. Feizi, Iron-doped TiO_2 catalysts with photocatalytic activity, J. Water Environ. Nanotechnol., 4 (2019) 60–66.

[11] M. Madadi, M. Ghorbanpour, A. Feizi, Preparation and characterization of solar light-induced rutile Cu-doped TiO_2 photocatalyst by solid-state molten salt method, Desal. Wat. Treat., 145 (2019) 257–261.

[12] T. Shahwan, Ç. Üzüm, A.E. Eroğlu, I. Lieberwirth, Synthesis and characterization of bentonite/iron nanoparticles and their applications adsorbent of cobalt ions, Appl. Clay Sci., 47 (2010) 257–262.

[13] A.A. Tireli, I. do Rosário Guimarães, J.C. de Souza Terra, R.R. da Silva, M.C. Guerreiro, Fenton-like processes and adsorption using iron oxide-pillared clay with magnetic properties for organic compound mitigation, Environ. Sci. Pollut. Res., 22 (2015) 870–881.

[14] T. Mishra, P. Mohapatra, K.M. Parida, Synthesis, characterisation and catalytic evaluation of iron–manganese mixed oxide pillared clay for VOC decomposition reaction, Appl. Catal., 79 (2008) 279–285.

[15] S. Louhichi, A. Ghorbel, H. Chekir, N. Trabelsi, S. Khemakhem, Properties of modified crude clay by iron and copper nanoparticles as potential hydrogen sulfide adsorption, Appl. Clay Sci., 127 (2016) 123–128.
[16] M. Ghorbanpour, Soybean oil bleaching by adsorption onto bentonite/iron oxide nanocomposites, *J*. Phys. Sci., 29 (2018) 113–119.
[17] S. Yamanaka, M. Hattori, Iron oxide pillared clay, Catal. Today, 2 (1988) 261–270.
[18] P. Yuan, H. He, F. Bergaya, D. Wu, Q. Zhou, J. Zhu, Synthesis and characterization of delaminated iron-pillared clay with meso–microporous structure, Microporous Mesoporous Mater., 88 (2006) 8–15.
[19] A. Nouri, M. Ghorbanpour, S. Lotfiman, Diffusion of Cu ions into nanoclay by molten salt ion exchange for antibacterial application, *J*. Phys. Sci., 29 (2018) 31–42.
[20] B. Hakimi, M. Ghorbanpour, A. Feizi, ZnO/bentonite nanocomposites prepared with solid-state ion exchange as photocatalysts, J. *Ultrafine Grained* Nanostruct. Mater., 51 (2018) 139–146.
[21] B. Hakimi, M. Ghorbanpour, A. Feizi, A comparative study between photocatalytic activity of ZnO/bentonite composites prepared by precipitation, liquid-state ion exchange and solid-state ion exchange Methods, J. Water Environ. Nanotechnol., 3 (2018) 273–278.
[22] Z.R. Liu, S.Q. Zhou, Adsorption of copper and nickel on Na-bentonite, Process Saf. Environ. Prot., 88 (2010) 62–66.
[23] H. Pouraboulghasem, M. Ghorbanpour, R. Shayegh, S. Lotfiman, Synthesis, characterization and antimicrobial activity of solid-state ion-exchanged ZnO/bentonite nanocomposites, J. Cent. Sout Univ. Technol., 23 (2016) 787–792.
[24] M. Ghorbanpour, M. Mazloumi, A. Nouri, Silver-doped nanoclay with antibacterial activity, J. *Ultrafine Grained* Nanostruct. Mater., 50 (2017) 124–131.
[25] M. Santhosh Kumar, M. Schwidder, W. Grünert, U. Bentrup, A. Brückner, Selective reduction of NO with Fe-ZSM-5 catalysts of low Fe content: part II. Assessing the function of different Fe sites by spectroscopic in situ studies, J. Catal., 239 (2006) 173–186.
[26] M. Schwidder, M.S. Kumar, K. Klementiev, M.M. Pohl, A. Brückner, W. Grünert, Selective reduction of NO with Fe-ZSM-5 catalysts of low Fe content I. Relations between active site structure and catalytic performance, J. Catal., 231 (2005) 314–330.
[27] M. Iwasaki, K. Yamazaki, K. Banno, H. Shinjoh, Characterization of Fe/ZSM-5 DeNO*x* catalysts prepared by different methods: relationships between active Fe sites and NH_3-SCR performance, J. Catal., 260 (2008) 205–216.
[28] Y. Gao, Y. Guo, H. Zhang, Iron modified bentonite: enhanced adsorption performance for organic pollutant and its regeneration by heterogeneous visible light photo-Fenton process at circumneutral pH, J. Hazard. Mater, 302 (2016) 105–113.
[29] K. Elass, A. Laachach, A. Alaoui, M. Azzi, Removal of methyl violet from aqueous solution using a stevensite-rich clay from Morocco, Appl. Clay Sci., 54 (2011) 90–96.